Electronic and Geometric Effects of Dual-Atom Catalysts on C−C Coupling during CO_2 Reduction: Insights from Density Functional Theory and Interpretable Machine Learning

Chenglong Qiu[1], Tore Brinck[2], and Jiacheng Wang[1,*]

[1] Zhejiang Key Laboratory for Island Green Energy and New Materials, Institute of Electrochemistry, School of Materials Science and Engineering, Taizhou University, Taizhou 318000, Zhejiang, China

[2] Department of Chemistry, CBH, KTH Royal Institute of Technology, SE-100 44 Stockholm, Sweden

Email: jiacheng.wang@tzc.edu.cn

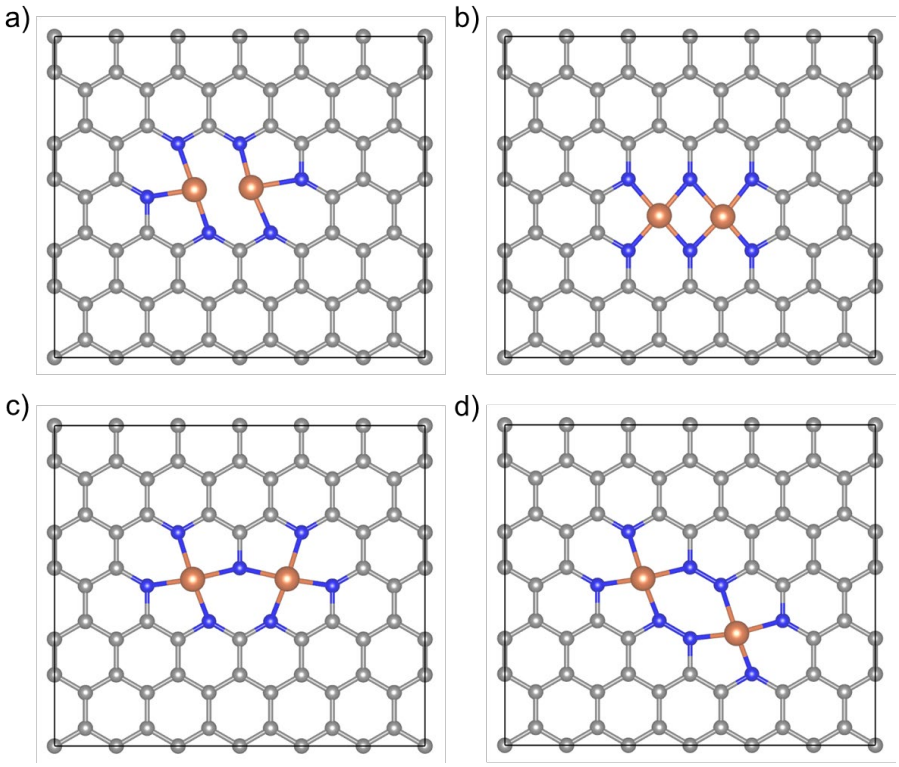

Figure S1. Four coordination configurations ($M_2@NG_1$, $M_2@NG_2$, $M_2@NG_3$, and $M_2@NG_4$) used in this work.

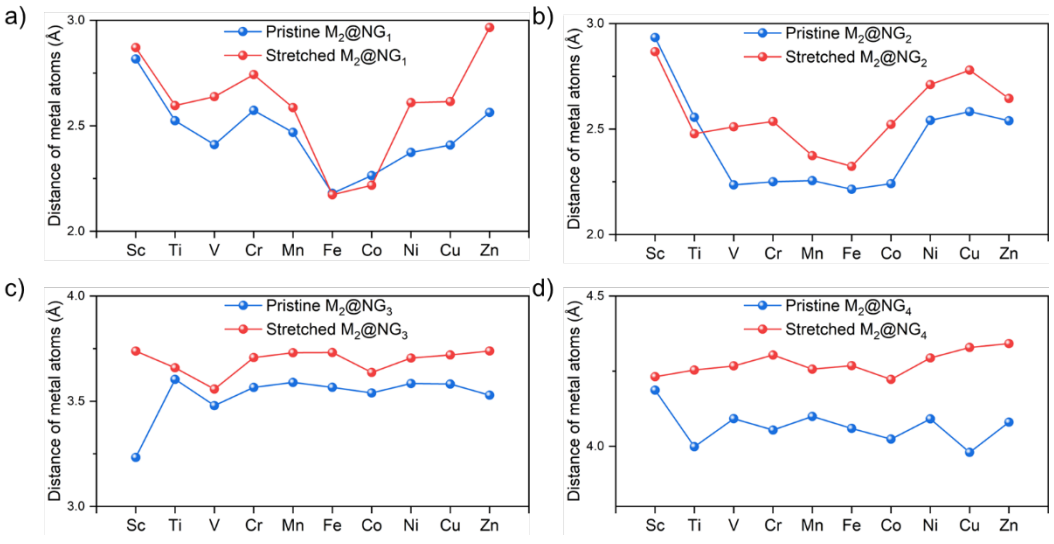

Figure S2. The distance of metal atoms before and after stretching for the four coordination structures

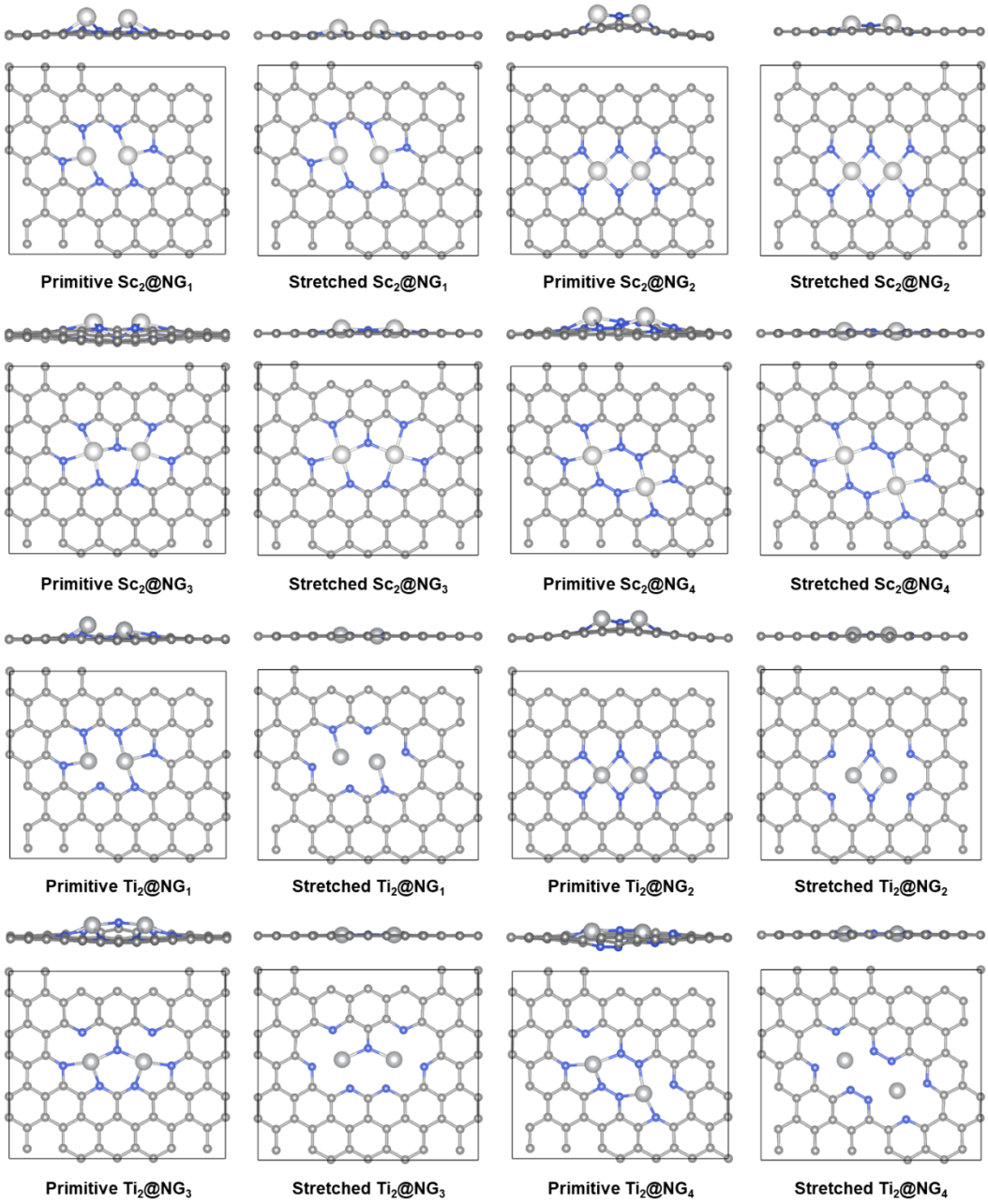

Figure S3. Optimized structures of $Sc_2@NG_x$ and $Ti_2@NG_x$ obtained from DFT calculations.

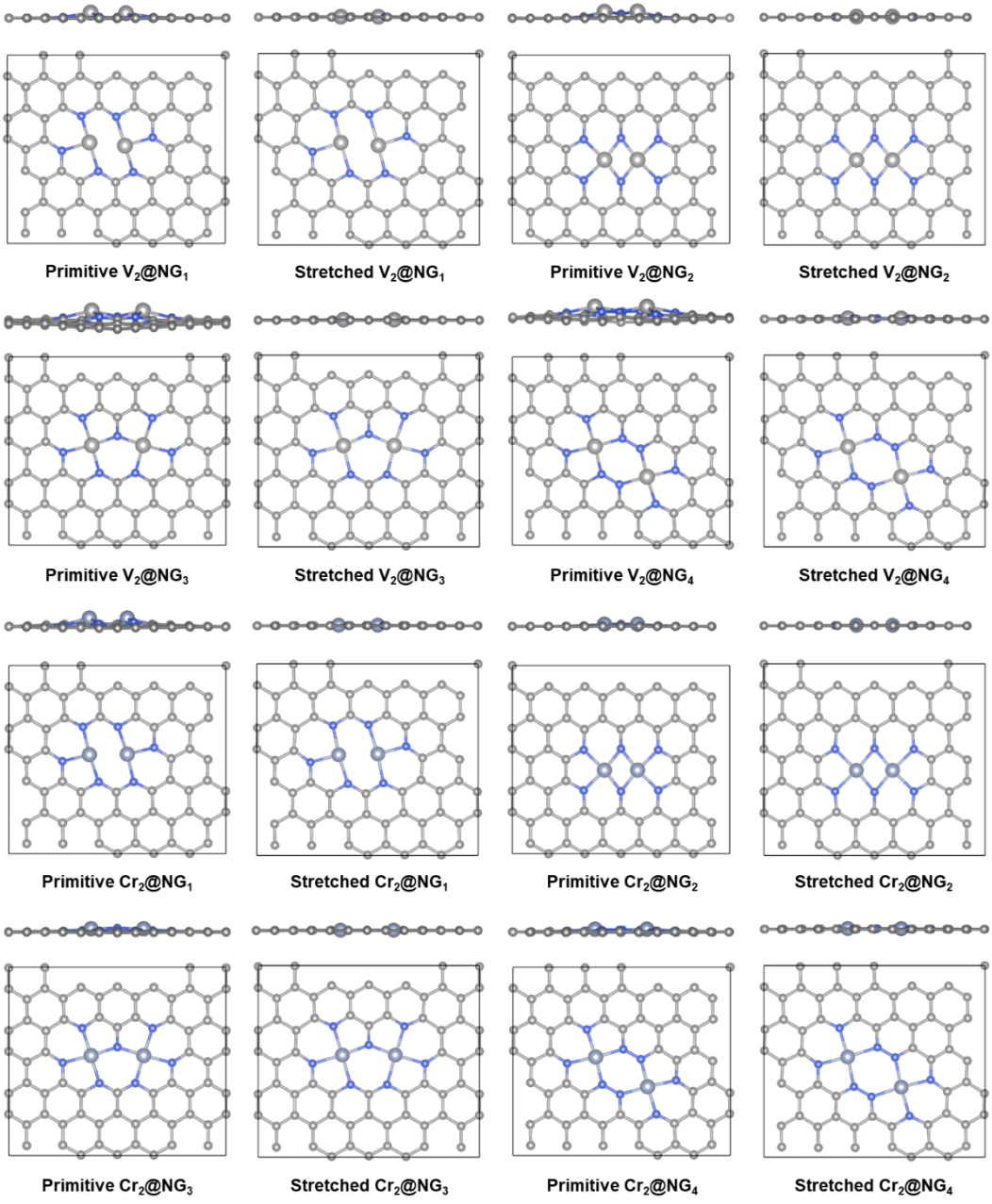

Figure S4. Optimized structures of $V_2@NG_x$ and $Cr_2@NG_x$ obtained from DFT calculations.

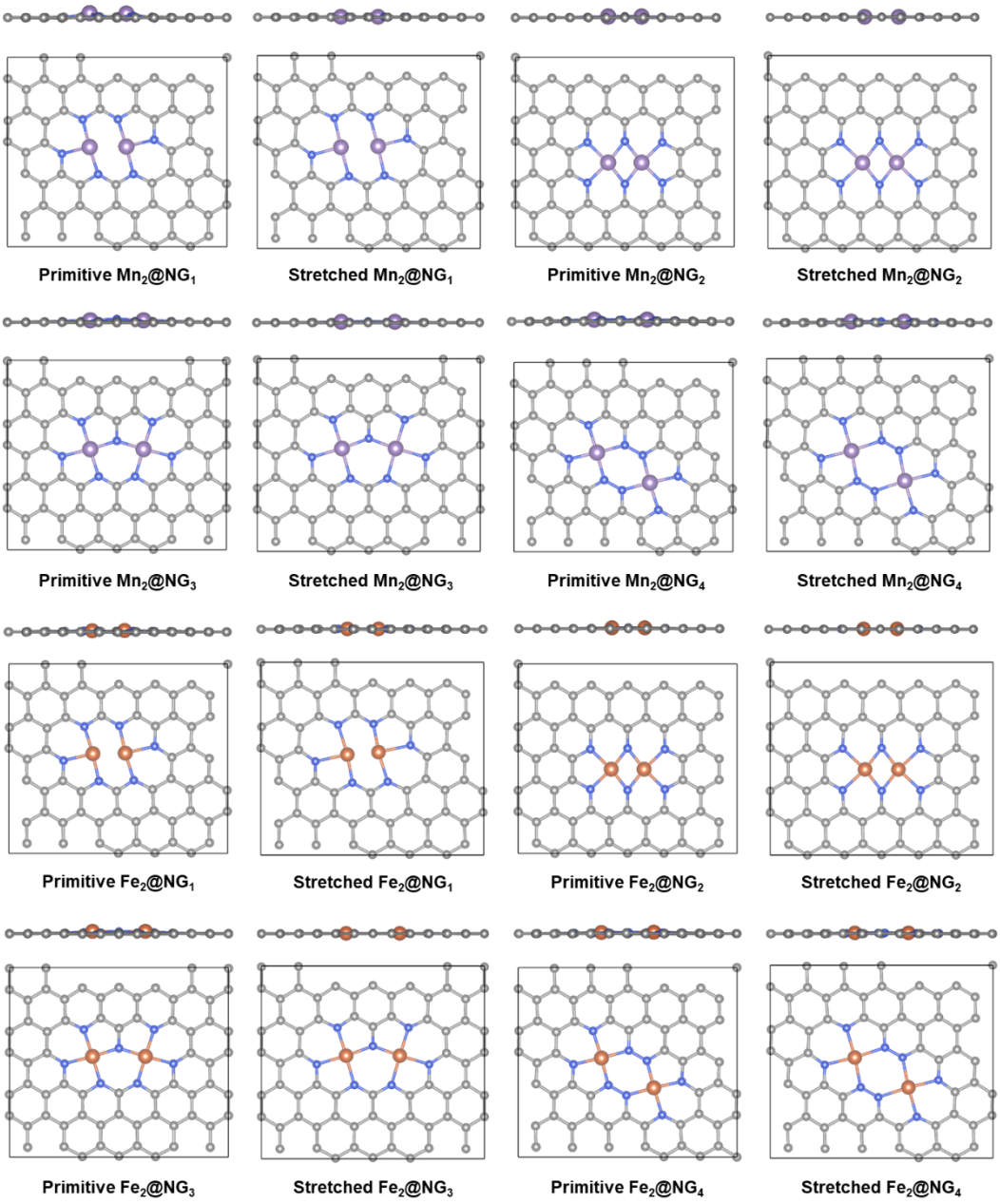

Figure S5. Optimized structures of $Mn_2@NG_x$ and $Fe_2@NG_x$ obtained from DFT calculations.

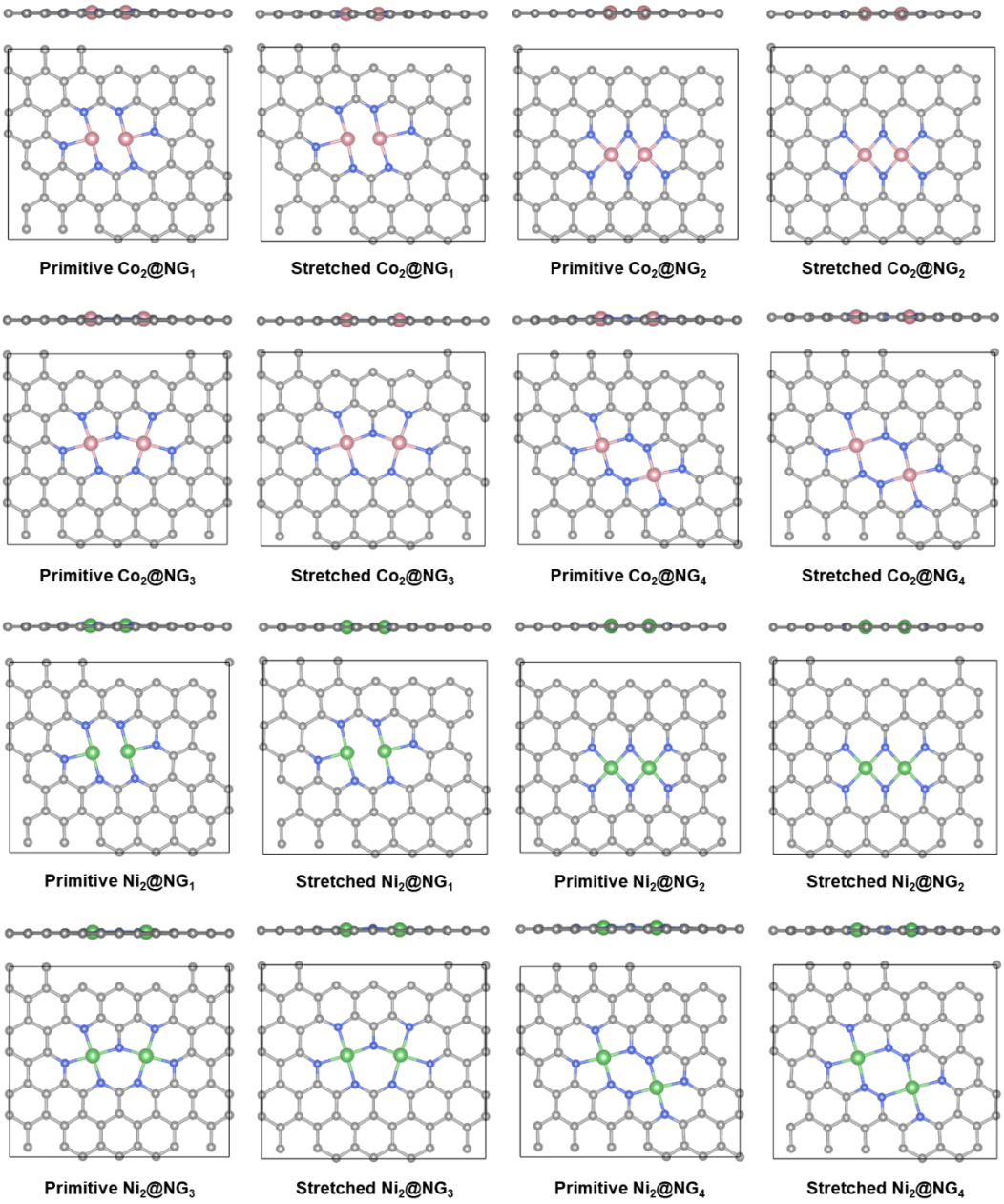

Figure S6. Optimized structures of $Co_2@NG_x$ and $Ni_2@NG_x$ obtained from DFT calculations.

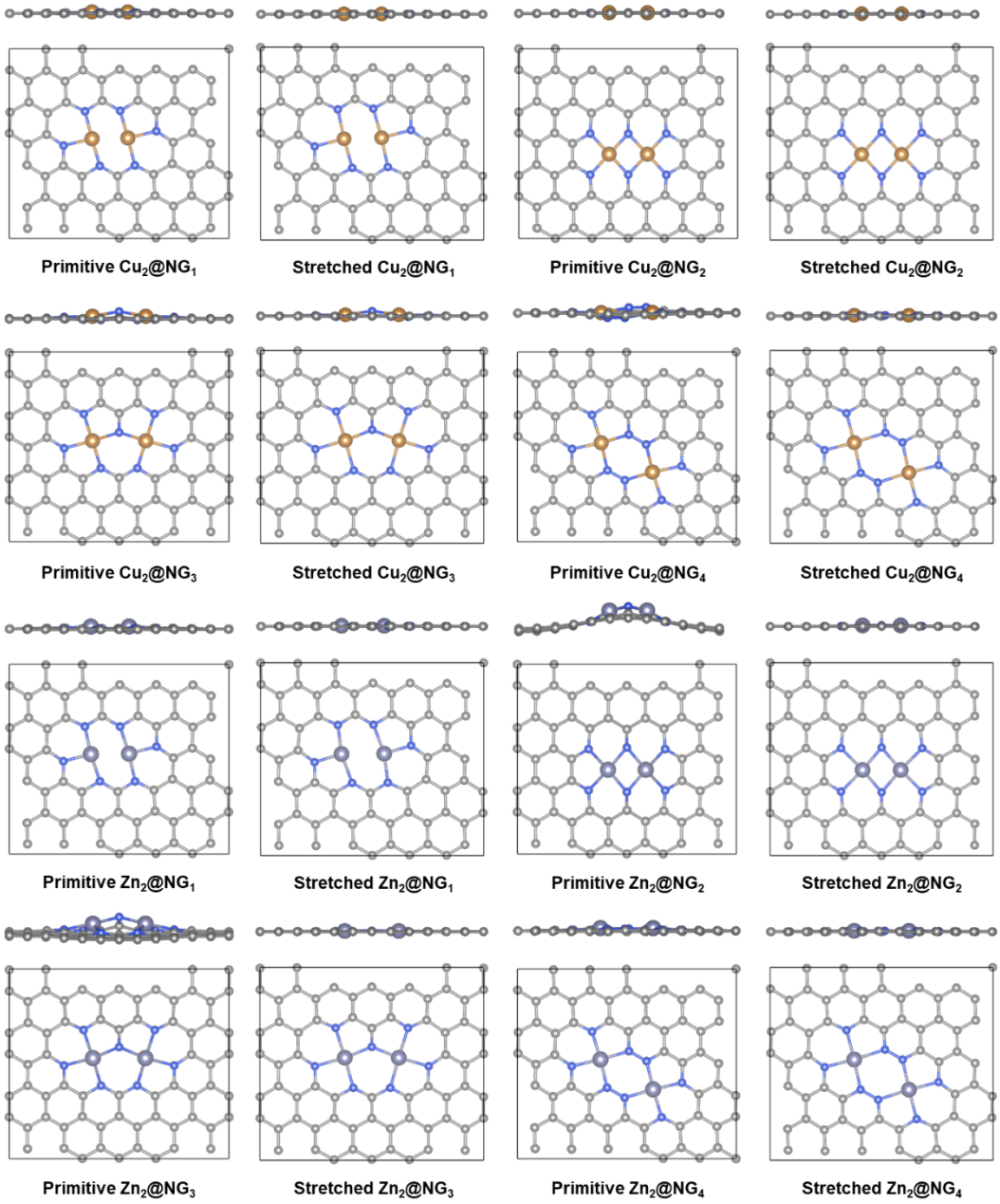

Figure S7. Optimized structures of $Cu_2@NG_x$ and $Zn_2@NG_x$ obtained from DFT calculations.

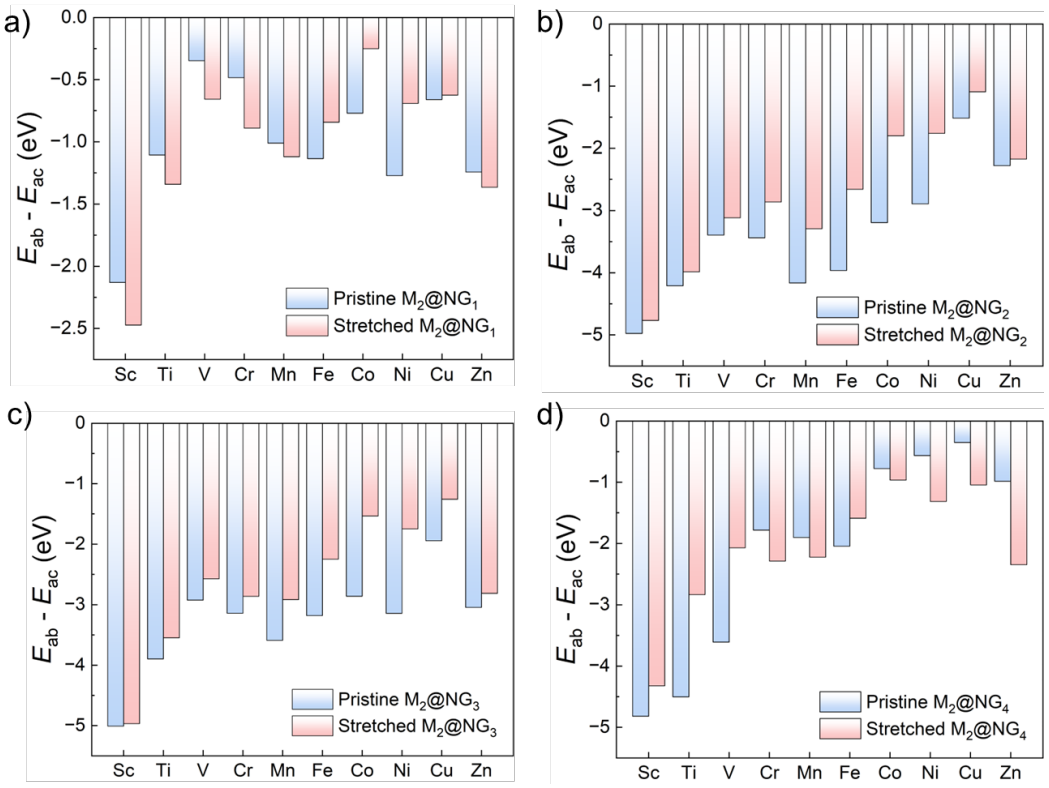

Figure S8. Differences between the average binding energies (E_{ab}) and the cohesive energies (E_{ac}) of a) M_2@NG_1, b) M_2@NG_2, c) M_2@NG_3 and d) M_2@NG_4.

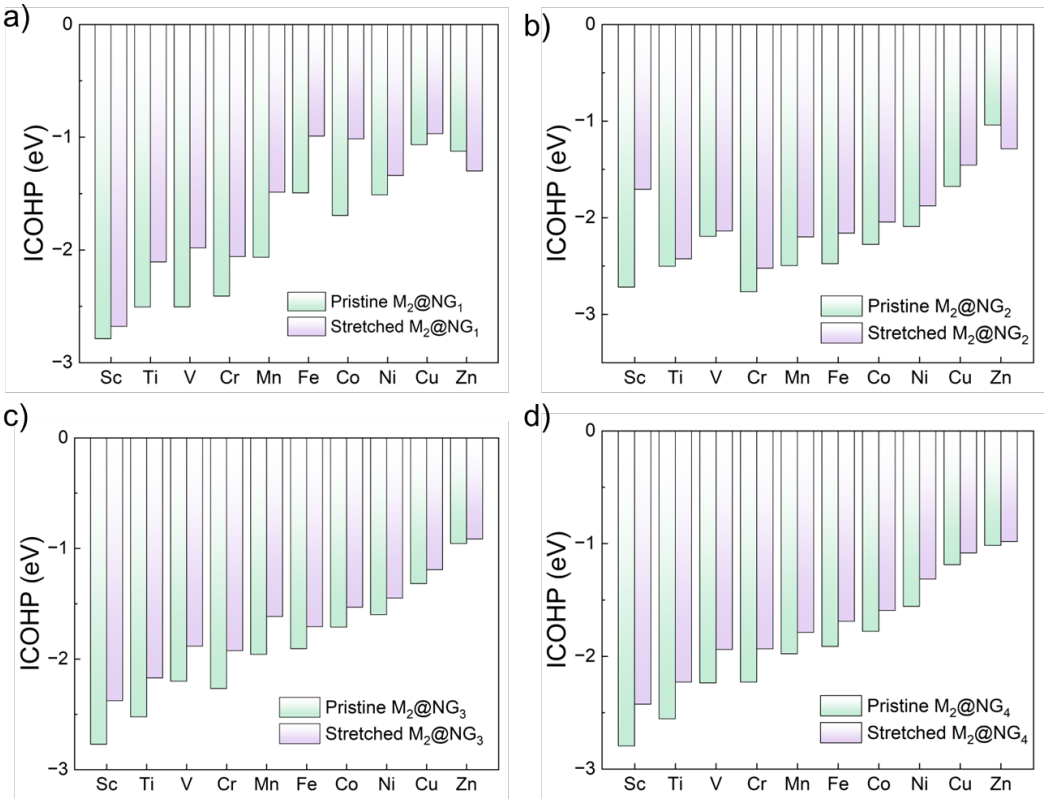

Figure S9. IpCOHPs values of the M−N bond in a) M_2@NG_1, b) M_2@NG_2, c) M_2@NG_3 and d) M_2@NG_4.

Table S1. The vibrational frequencies (THz) of the dual-atom sites in $Sc_2@NG_x$.

Mode	Primitive $Sc_2@NG_1$	Stretched $Sc_2@NG_1$	Primitive $Sc_2@NG_2$	Stretched $Sc_2@NG_2$	Primitive $Sc_2@NG_3$	Stretched $Sc_2@NG_3$	Primitive $Sc_2@NG_4$	Stretched $Sc_2@NG_4$
1	9.316773	9.004974	10.920667	11.004719	10.166779	10.099946	9.607972	8.442071
2	8.967372	7.738182	10.347725	10.134674	9.326864	8.640436	9.392005	8.362029
3	7.71301	7.301387	8.383973	7.445307	9.033565	8.570755	8.635332	7.634694
4	6.996057	6.77365	7.966135	5.830091	8.881757	7.556193	8.628472	7.480081
5	5.993831	3.18848	7.222447	4.544677	7.444548	2.839287	7.38396	2.185778
6	4.011628	2.299929	5.611131	0.915953	7.117348	2.01292	7.183701	1.106289

Table S2. The vibrational frequencies (THz) of the dual-atom sites in $Ti_2@NG_x$.

Mode	Primitive $Ti_2@NG_1$	Stretched $Ti_2@NG_1$	Primitive $Ti_2@NG_2$	Stretched $Ti_2@NG_2$	Primitive $Ti_2@NG_3$	Stretched $Ti_2@NG_3$	Primitive $Ti_2@NG_4$	Stretched $Ti_2@NG_4$
1	10.57387	9.84755	12.56294	12.78372	10.32801	9.213594	10.59982	7.658709
2	9.694974	8.923023	11.77867	10.37232	9.287821	8.22969	10.36844	7.294945
3	7.816784	7.882945	9.955684	8.784915	9.210605	7.482461	10.27165	6.40705
4	7.569598	5.097188	8.178171	7.692146	8.348985	5.098973	10.02448	6.058661
5	5.557177	2.889661	7.187455	3.087299	5.643901	3.031698	6.472319	4.261046
6	3.133584	1.604609	5.403919	2.395648	5.60383	2.686022	6.262583	4.088917

Table S3. The vibrational frequencies (THz) of the dual-atom sites in $V_2@NG_x$.

Mode	Primitive $V_2@NG_1$	Stretched $V_2@NG_1$	Primitive $V_2@NG_2$	Stretched $V_2@NG_2$	Primitive $V_2@NG_3$	Stretched $V_2@NG_3$	Primitive $V_2@NG_4$	Stretched $V_2@NG_4$
1	12.05213	9.238933	16.50098	12.66636	11.5156	9.810043	10.89707	8.847403
2	11.48185	8.700731	13.66681	9.941802	10.62282	9.040535	10.81714	8.695482
3	11.23423	7.78796	13.43959	7.687982	8.98066	7.125997	9.264744	7.423337
4	7.806956	6.122759	10.97417	6.695414	8.68685	5.916034	9.176639	6.513621
5	2.454013	3.578786	4.397134	4.815498	5.799825	4.148066	5.504205	4.496506
6	0.938059	3.333083	3.482074	4.224605	5.615928	2.646662	5.249116	4.355659

Table S4. The vibrational frequencies (THz) of the dual-atom sites in $Cr_2@NG_x$.

Mode	Primitive $Cr_2@NG_1$	Stretched $Cr_2@NG_1$	Primitive $Cr_2@NG_2$	Stretched $Cr_2@NG_2$	Primitive $Cr_2@NG_3$	Stretched $Cr_2@NG_3$	Primitive $Cr_2@NG_4$	Stretched $Cr_2@NG_4$
1	11.55152	9.64191	16.46828	12.45979	12.68443	9.551832	12.88626	8.656729
2	10.78657	8.316507	13.71297	9.189695	12.22443	9.016957	12.21739	8.409364
3	10.76054	8.068488	13.23759	7.206016	11.39507	7.925769	10.84024	7.041526
4	8.510663	6.809016	12.01326	6.562672	10.56674	7.231154	10.37024	6.960596
5	3.353542	4.183344	5.050871	5.328826	3.778072	4.959091	4.012748	4.893311
6	3.306587	3.407458	4.701359	4.756068	2.501537	4.543083	3.860774	4.886183

Table S5. The vibrational frequencies (THz) of the dual-atom sites in $Mn_2@NG_x$.

Mode	Primitive $Mn_2@NG_1$	Stretched $Mn_2@NG_1$	Primitive $Mn_2@NG_2$	Stretched $Mn_2@NG_2$	Primitive $Mn_2@NG_3$	Stretched $Mn_2@NG_3$	Primitive $Mn_2@NG_4$	Stretched $Mn_2@NG_4$
1	10.86654	7.862315	16.57839	12.60194	12.24445	8.515272	11.9876	6.82488
2	10.60497	7.187056	12.8523	9.351011	11.89726	7.540964	11.9135	6.44016
3	10.17618	6.696281	12.22789	8.942024	10.74434	7.280371	10.5583	5.482239
4	7.63876	5.50257	11.88918	8.814127	9.432718	6.643935	9.785567	5.3378
5	2.857413	3.484858	5.024171	6.1248	4.211132	3.969435	4.867312	2.949774
6	0.72284	3.432592	4.769059	5.561691	3.929061	3.827151	4.836321	2.904429

Table S6. The vibrational frequencies (THz) of the dual-atom sites in $Fe_2@NG_x$.

Mode	Primitive $Fe_2@NG_1$	Stretched $Fe_2@NG_1$	Primitive $Fe_2@NG_2$	Stretched $Fe_2@NG_2$	Primitive $Fe_2@NG_3$	Stretched $Fe_2@NG_3$	Primitive $Fe_2@NG_4$	Stretched $Fe_2@NG_4$
1	12.52592	9.408333	16.65699	12.0361	13.48897	9.739596	13.59748	7.534686
2	11.08915	7.145488	12.55452	9.036042	12.73553	9.194515	13.58504	7.523792
3	6.870096	7.044325	12.18538	8.582297	10.61913	7.01274	10.05335	4.813346
4	3.823523	4.88875	11.98792	8.17323	10.09213	6.620564	9.343369	4.605142
5	3.692554	4.357122	7.385604	7.11841	4.396967	5.212062	5.081951	4.287425
6	1.147994	3.749691	7.073005	6.725654	0.430856	5.070294	5.033175	3.643457

Table S7. The vibrational frequencies (THz) of the dual-atom sites in $Co_2@NG_x$.

Mode	Primitive $Co_2@NG_1$	Stretched $Co_2@NG_1$	Primitive $Co_2@NG_2$	Stretched $Co_2@NG_2$	Primitive $Co_2@NG_3$	Stretched $Co_2@NG_3$	Primitive $Co_2@NG_4$	Stretched $Co_2@NG_4$
1	12.25184	7.973211	15.31767	10.34512	12.87272	8.720521	12.61556	7.832804
2	10.58849	6.155043	11.4719	8.525775	12.6219	8.344646	12.45573	7.711905
3	8.005698	5.590508	11.4003	6.594846	9.569304	6.165051	9.01337	5.57976
4	6.472915	4.361715	10.62435	6.503735	9.534731	5.798231	8.74454	5.447677
5	5.081186	3.829767	7.165859	6.28848	5.944415	5.416226	6.248193	4.740993
6	4.451782	3.370782	6.742883	5.322084	5.492194	5.2184	6.085859	4.604444

Table S8. The vibrational frequencies (THz) of the dual-atom sites in $Ni_2@NG_x$.

Mode	Primitive $Ni_2@NG_1$	Stretched $Ni_2@NG_1$	Primitive $Ni_2@NG_2$	Stretched $Ni_2@NG_2$	Primitive $Ni_2@NG_3$	Stretched $Ni_2@NG_3$	Primitive $Ni_2@NG_4$	Stretched $Ni_2@NG_4$
1	12.11077	7.913031	13.97522	10.15489	12.69963	8.277956	12.48194	5.95907
2	10.63264	6.950327	12.72472	9.226938	12.45616	7.972587	12.46924	5.952822
3	9.329102	5.145016	10.27307	6.63179	9.699919	6.023008	9.159387	4.41323
4	7.608156	4.884669	9.26779	6.212425	9.63718	5.906755	9.070503	4.286687
5	5.787589	4.645035	6.174984	6.18548	6.346794	5.83761	6.490681	3.33988
6	4.658919	4.225215	5.540971	4.690916	6.258009	5.727869	6.398068	3.314725

Table S9. The vibrational frequencies (THz) of the dual-atom sites in $Cu_2@NG_x$.

Mode	Primitive $Cu_2@NG_1$	Stretched $Cu_2@NG_1$	Primitive $Cu_2@NG_2$	Stretched $Cu_2@NG_2$	Primitive $Cu_2@NG_3$	Stretched $Cu_2@NG_3$	Primitive $Cu_2@NG_4$	Stretched $Cu_2@NG_4$
1	9.936794	6.127416	12.24375	7.443796	10.29422	6.657212	9.197751	5.462936
2	9.599072	5.675037	11.29278	7.329438	10.28591	6.427868	9.138364	5.455046
3	8.399326	4.511814	9.684853	4.993669	8.653567	4.763444	7.054827	3.74592
4	6.447607	3.881612	8.947376	4.849834	8.551016	4.559822	6.940967	3.727867
5	3.872885	3.809835	4.524553	4.16503	4.735718	4.38332	3.831015	3.500767
6	3.213826	3.436775	4.35147	4.083826	4.712221	4.217466	3.205325	3.393084

Table S10. The vibrational frequencies (THz) of the dual-atom sites in $Zn_2@NG_x$.

Mode	Primitive $Zn_2@NG_1$	Stretched $Zn_2@NG_1$	Primitive $Zn_2@NG_2$	Stretched $Zn_2@NG_2$	Primitive $Zn_2@NG_3$	Stretched $Zn_2@NG_3$	Primitive $Zn_2@NG_4$	Stretched $Zn_2@NG_4$
1	9.93665	7.34519	8.661405	7.493182	8.488067	6.920357	8.916262	5.951318
2	9.708174	7.28671	7.235698	6.131473	8.266858	6.640684	8.806532	5.866168
3	8.488516	5.532864	6.826001	5.78292	6.713467	4.685273	7.404447	4.332158
4	7.195947	5.462043	6.5276	5.390046	6.367172	4.318999	7.34738	4.208906
5	2.402408	3.286837	3.628901	3.761667	3.738533	3.81539	2.647068	3.668372
6	1.880129	2.893935	2.788773	3.193196	3.584572	3.793533	2.520754	3.603826

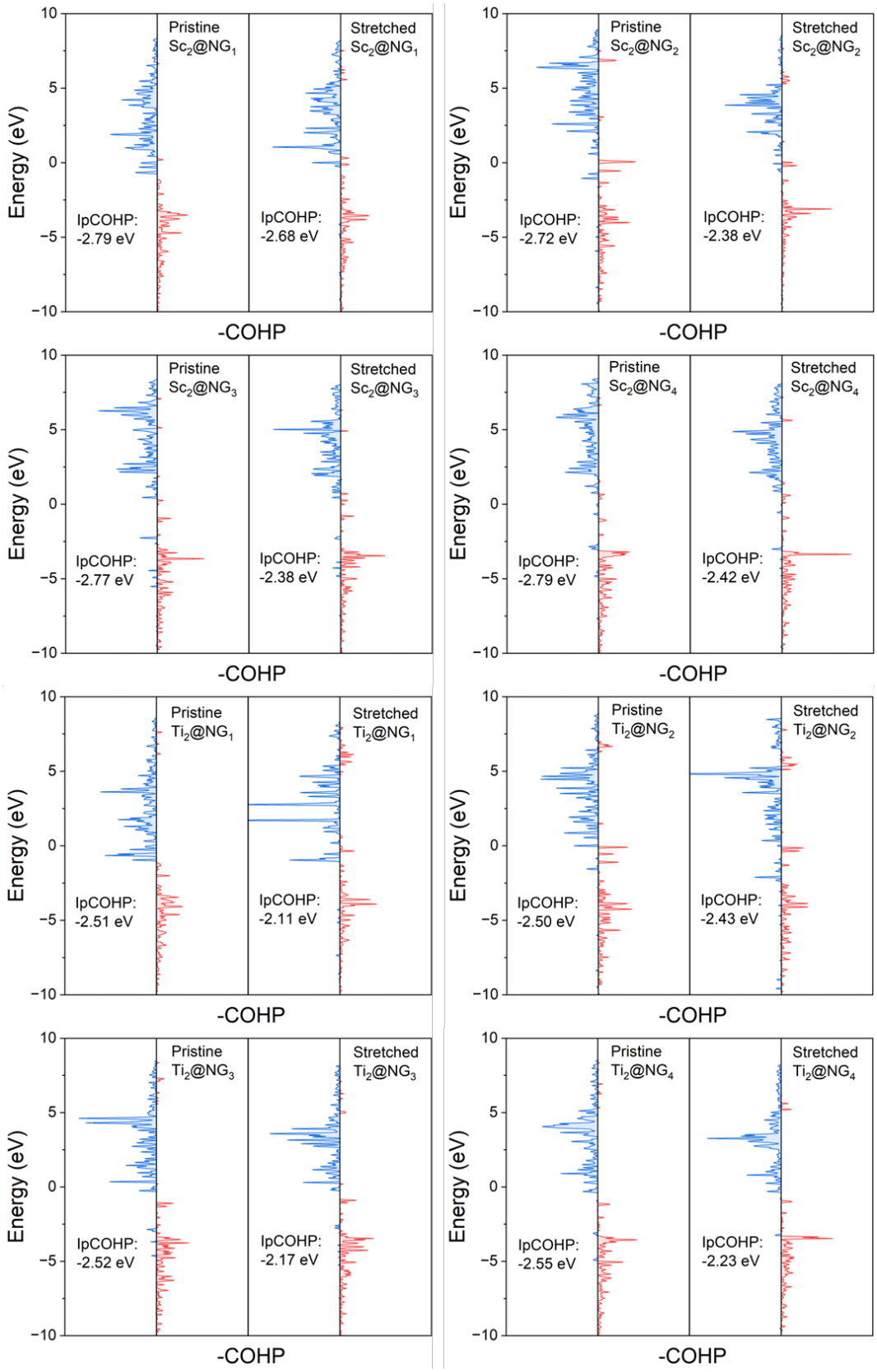

Figure S10. COHP curves of the M−N bond in $Sc_2@NG_x$ and $Ti_2@NG_x$.

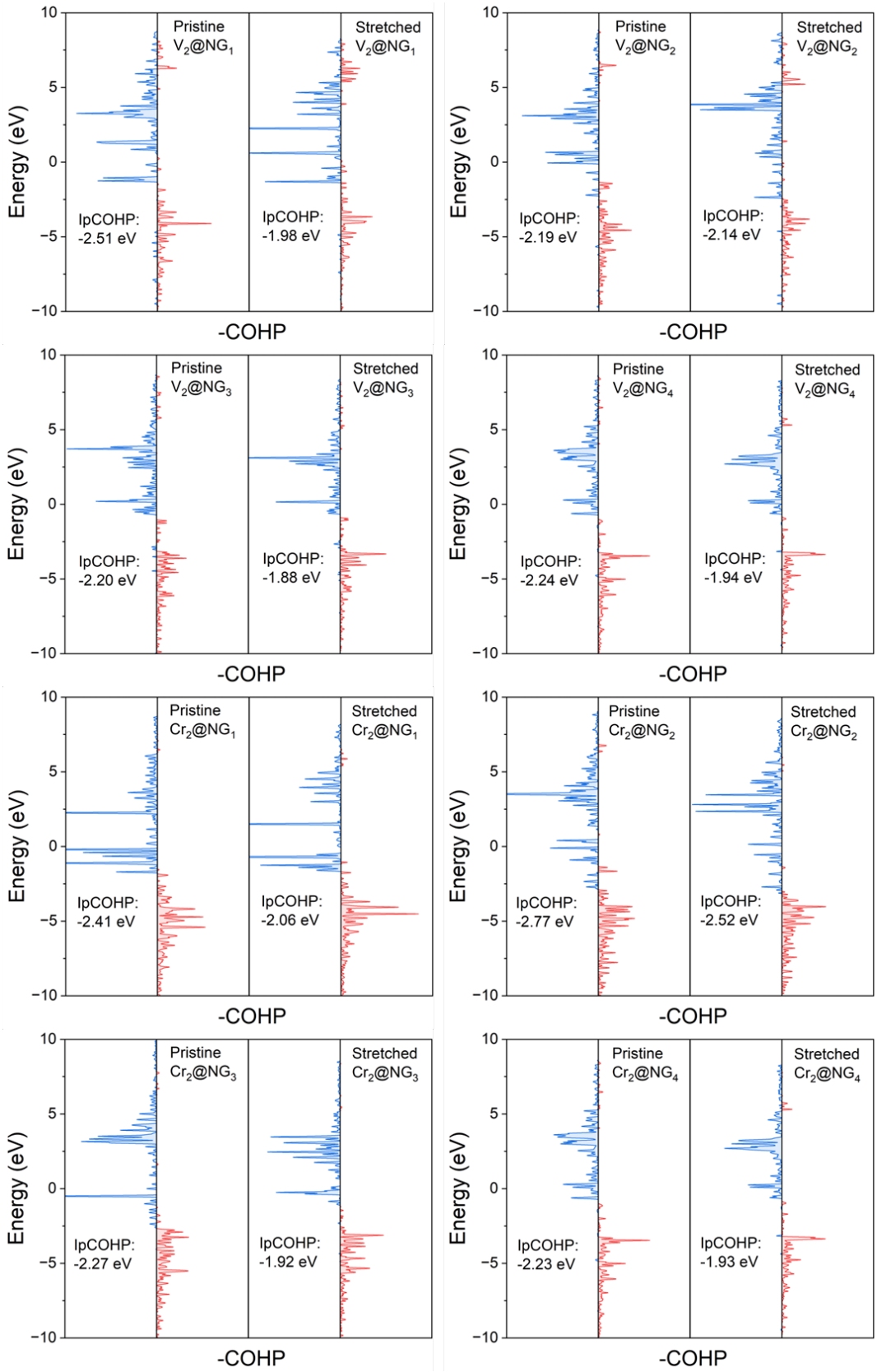

Figure S11. COHP curves of the M−N bond in $V_2@NG_x$ and $Cr_2@NG_x$.

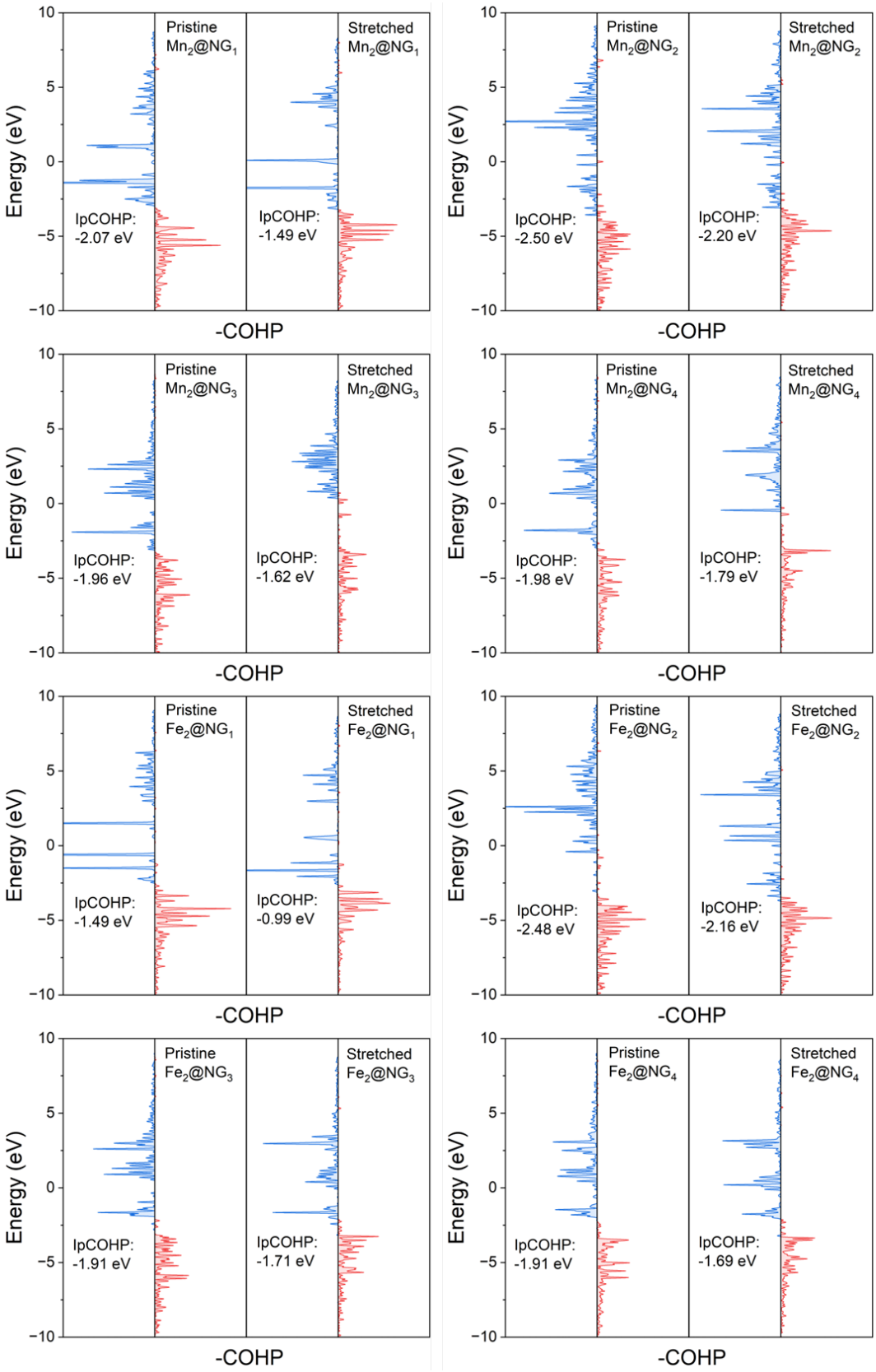

Figure S12. COHP curves of the M−N bond in $Mn_2@NG_x$ and $Fe_2@NG_x$.

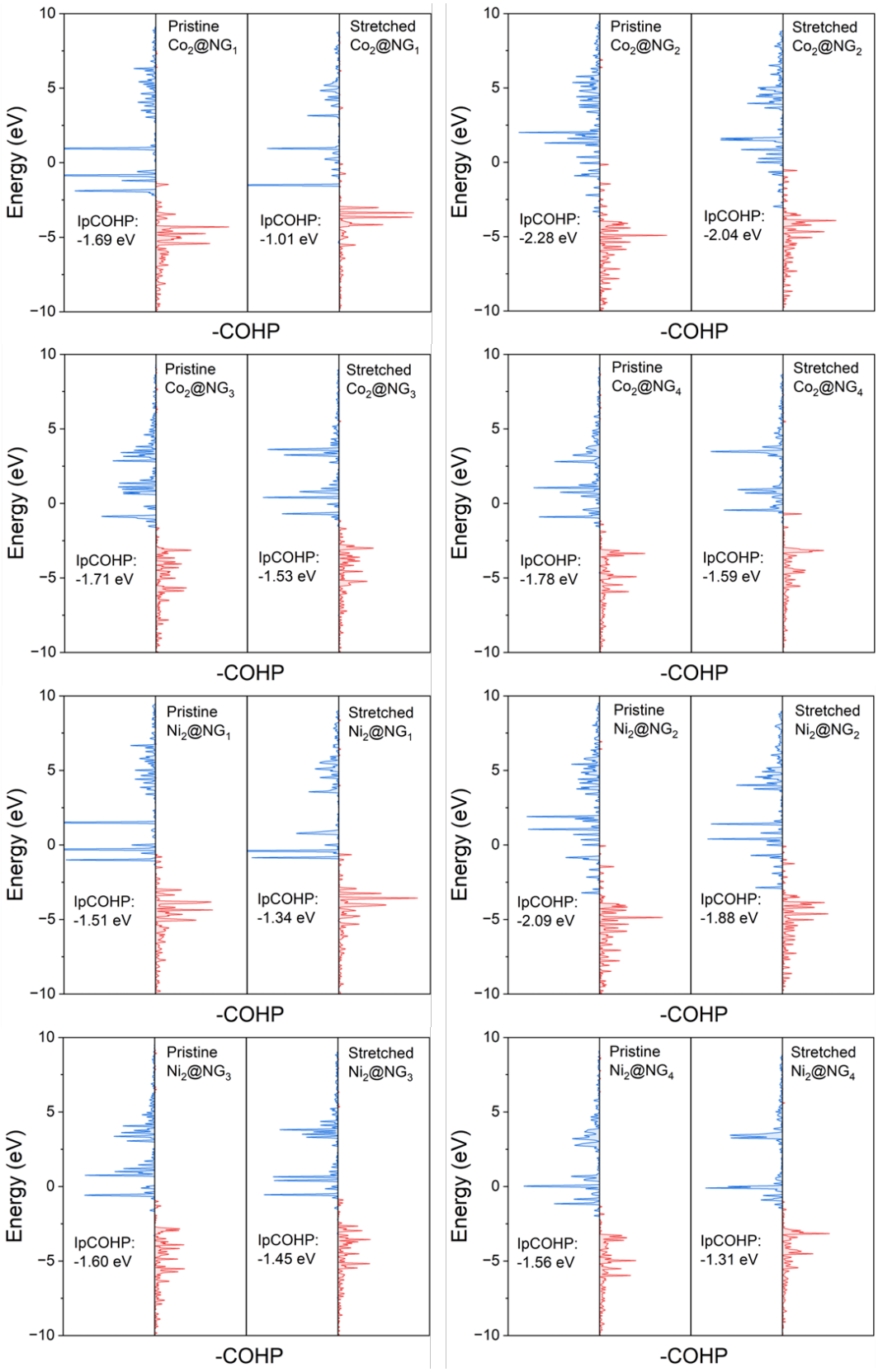

Figure S13. COHP curves of the M−N bond in $Co_2@NG_x$ and $Ni_2@NG_x$.

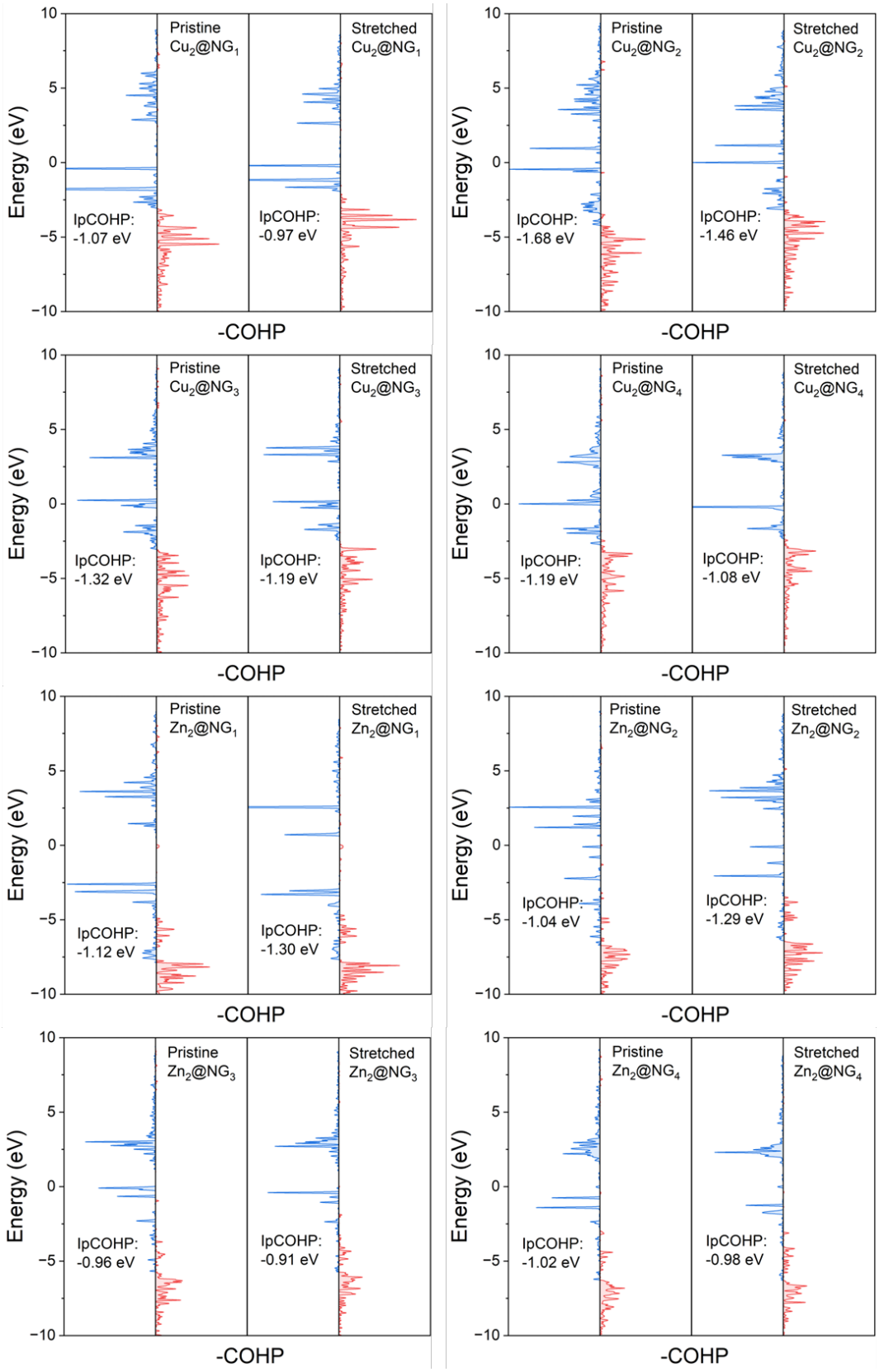

Figure S14. COHP curves of the M−N bond in $Cu_2@NG_x$ and $Zn_2@NG_x$.

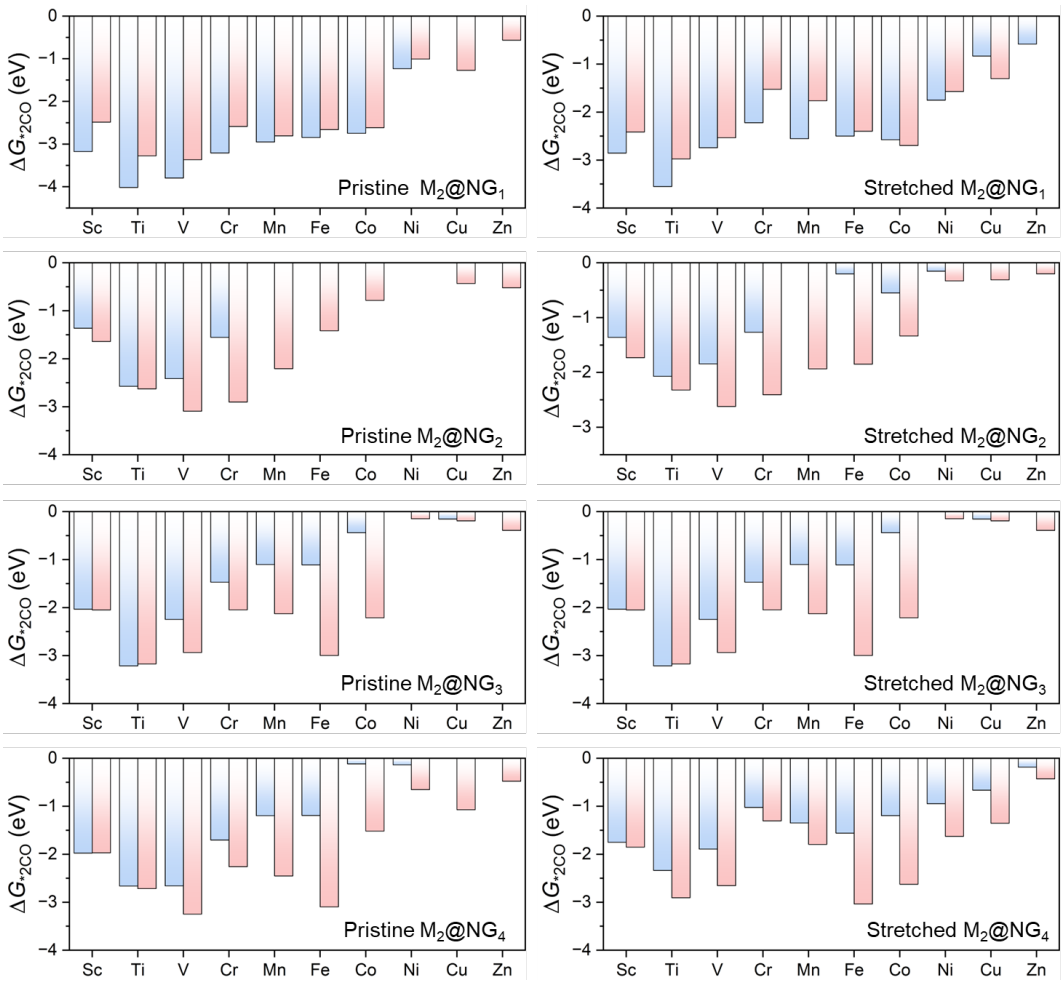

Figure S15. Adsorption energies of two CO molecules on $M_2@NG_x$ in top−bridged (blue bars) and top−top (red bars) configurations.

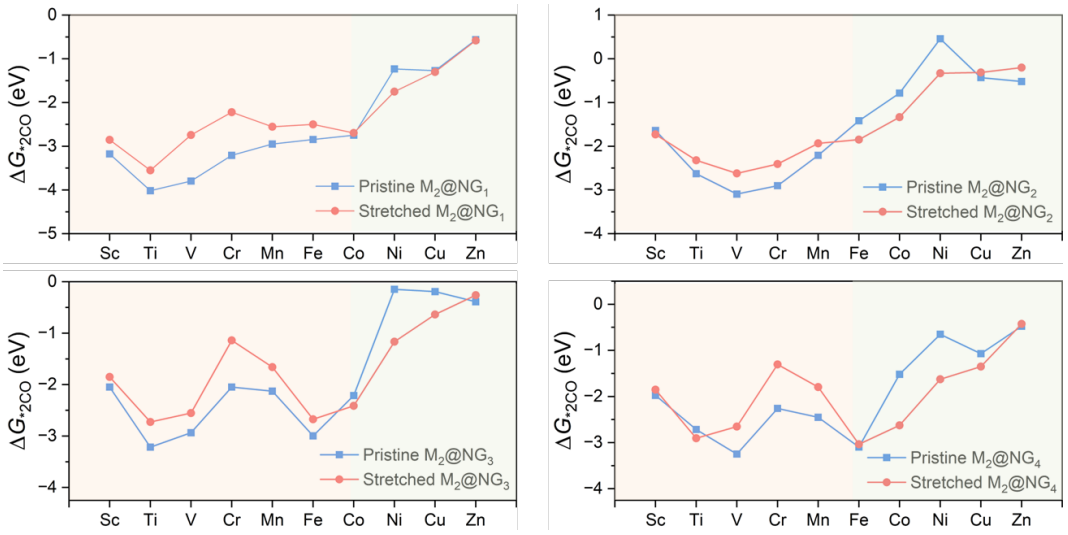

Figure S16. Comparison of the most stable adsorption energies of two CO molecules on pristine $M_2@NG_x$ and stretched $M_2@NG_x$.

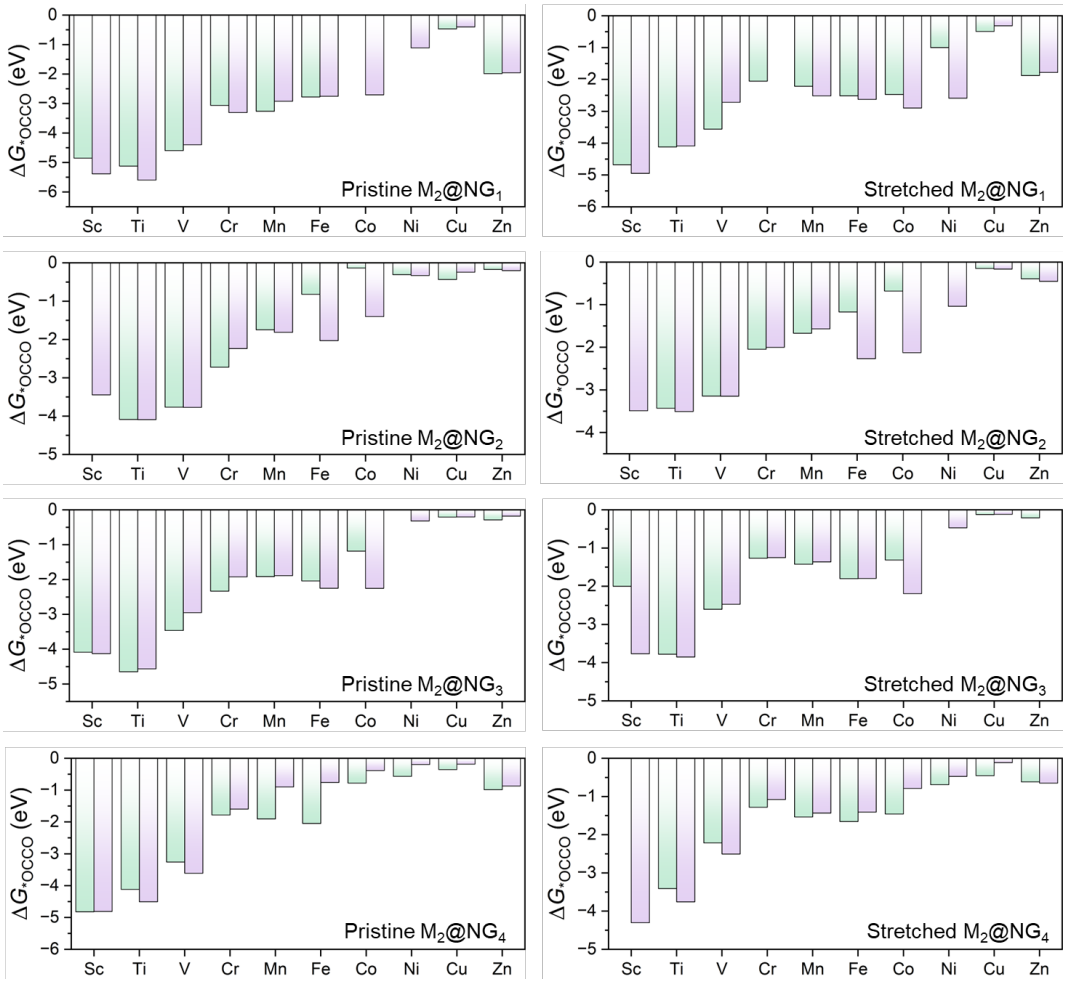

Figure S17. Adsorption energies of *OCCO molecules on $M_2@NG_x$ with single-site (green bars) and dual-site (purple bars) configurations.

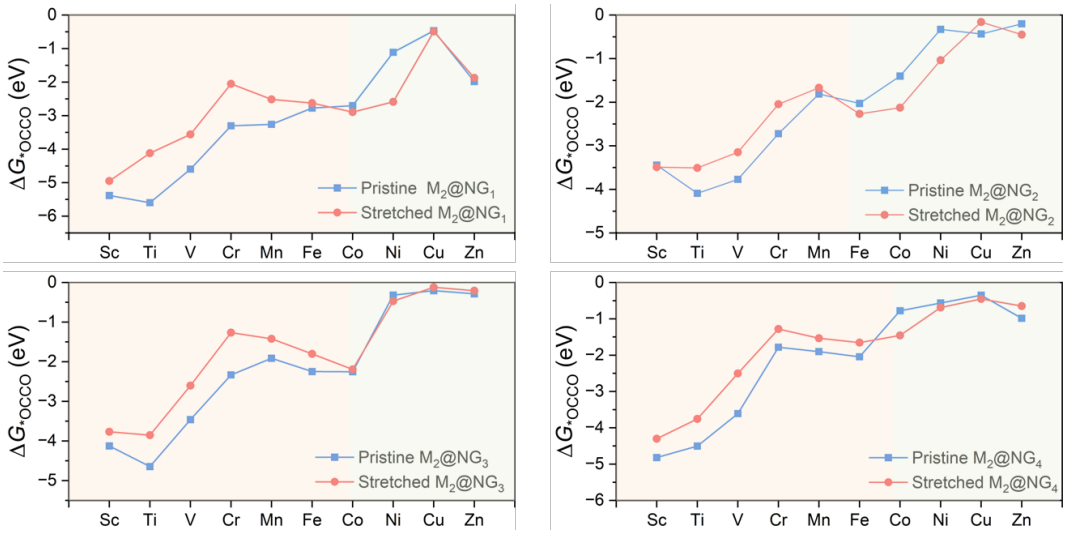

Figure S18. Comparison of the most stable adsorption energies of *OCCO molecules on pristine $M_2@NG_x$ and stretched $M_2@NG_x$.

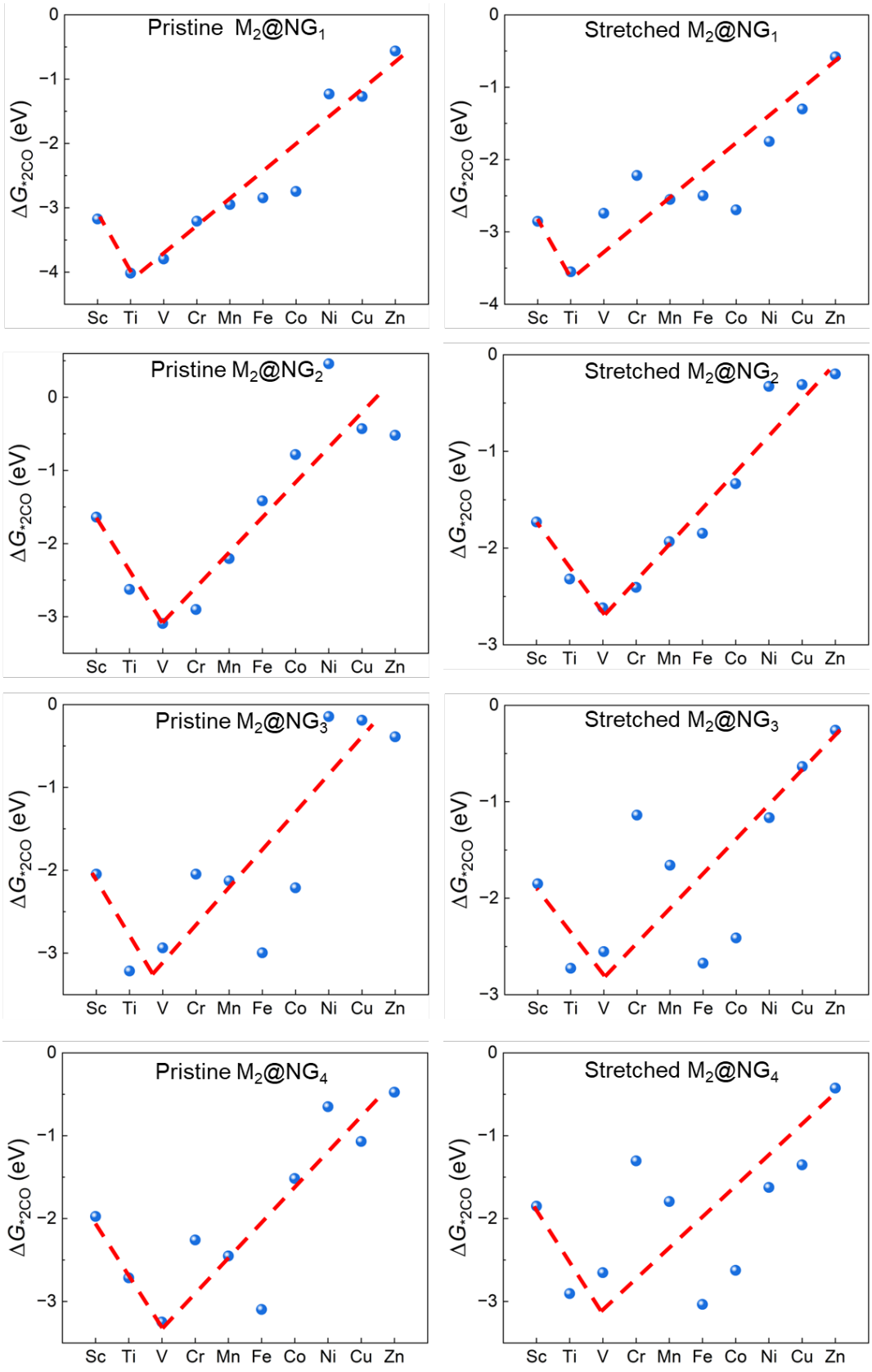

Figure S19. Adsorption energies of two CO molecules as a function of metal identity in $M_2@NG_x$.

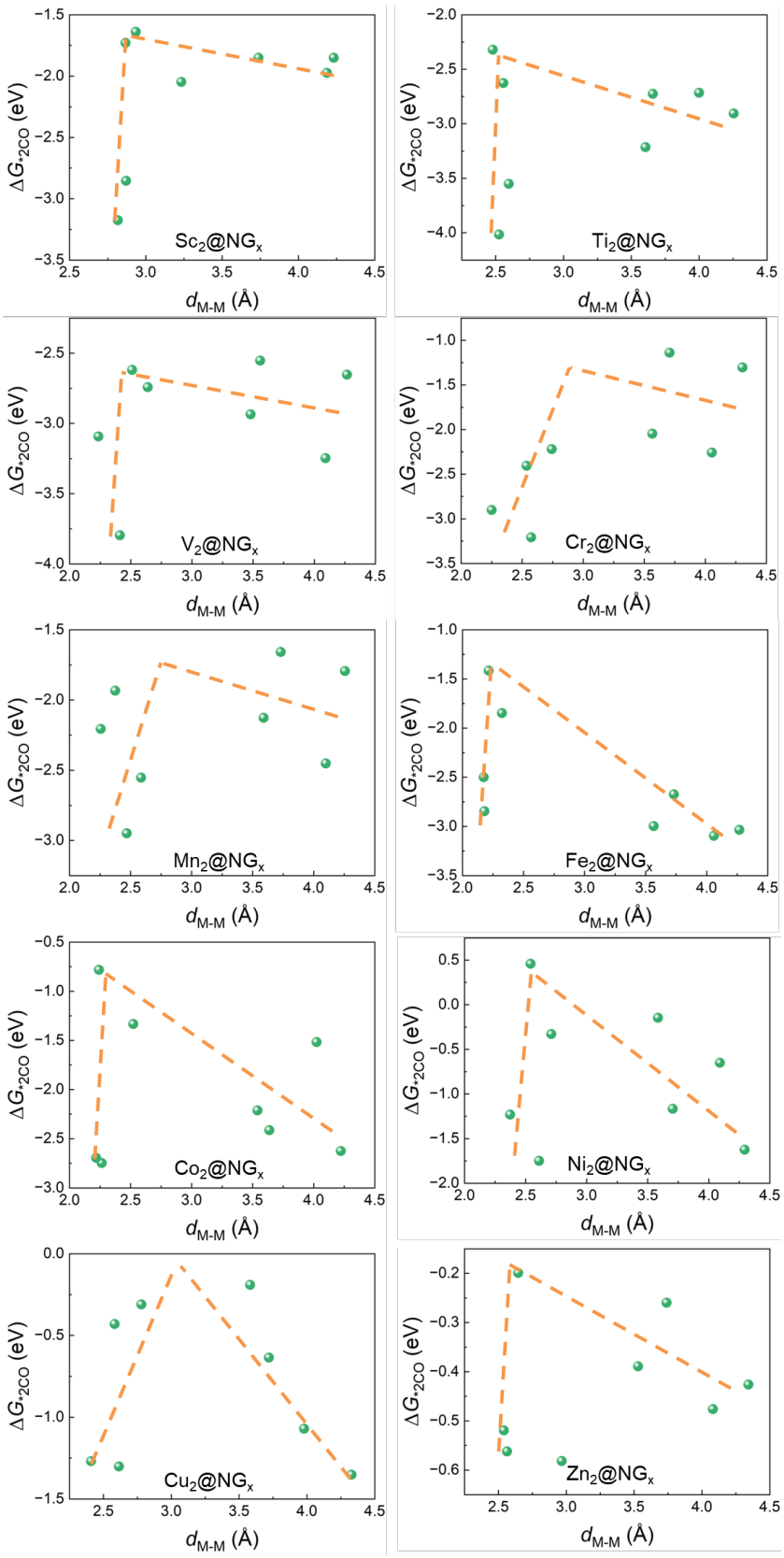

Figure S20. Adsorption energies of two CO molecules as a function of metal−metal distance in $M_2@NG_x$.

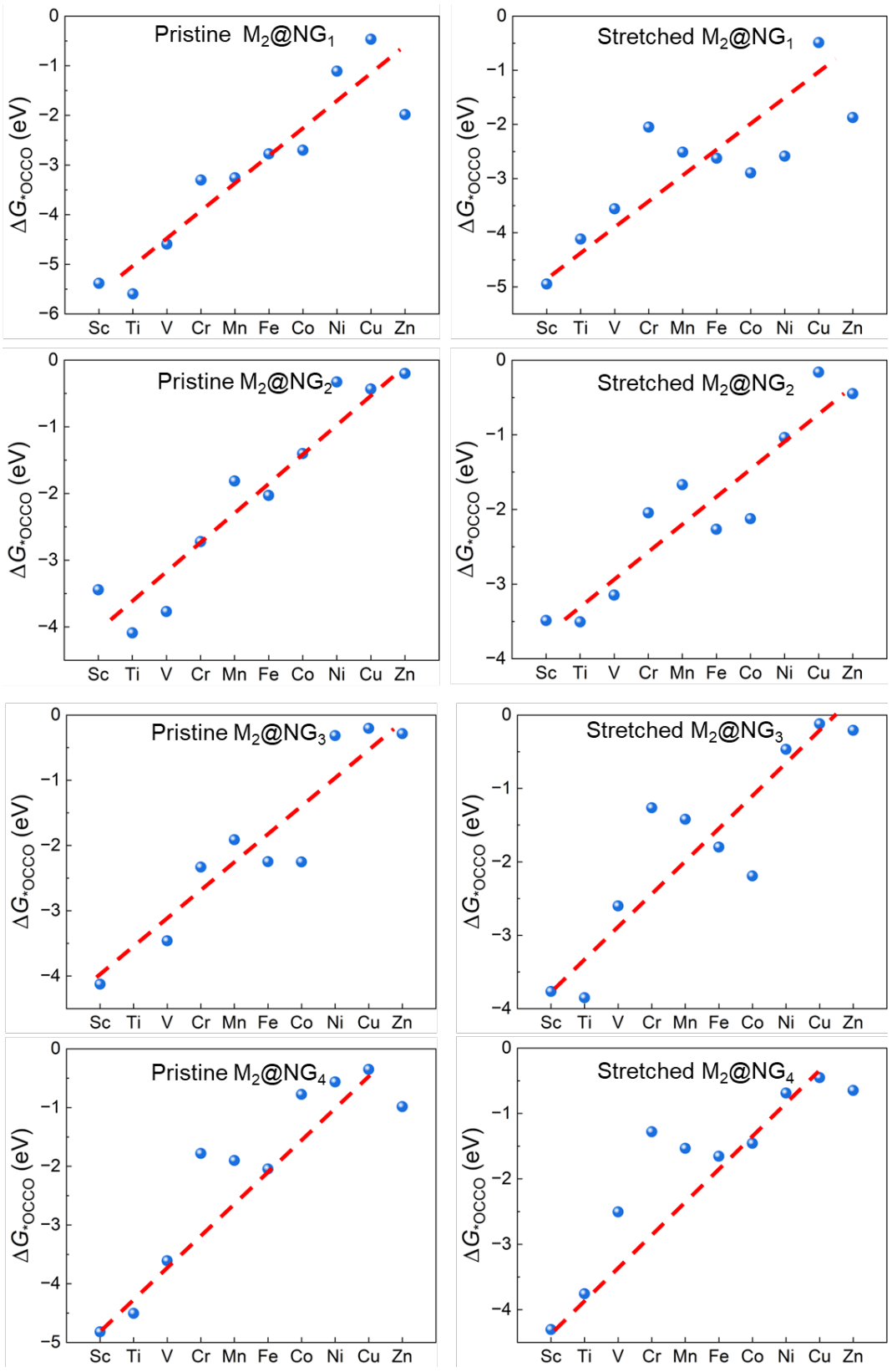

Figure S21. Adsorption energies of *OCCO molecules as a function of metal identity in $M_2@NG_x$.

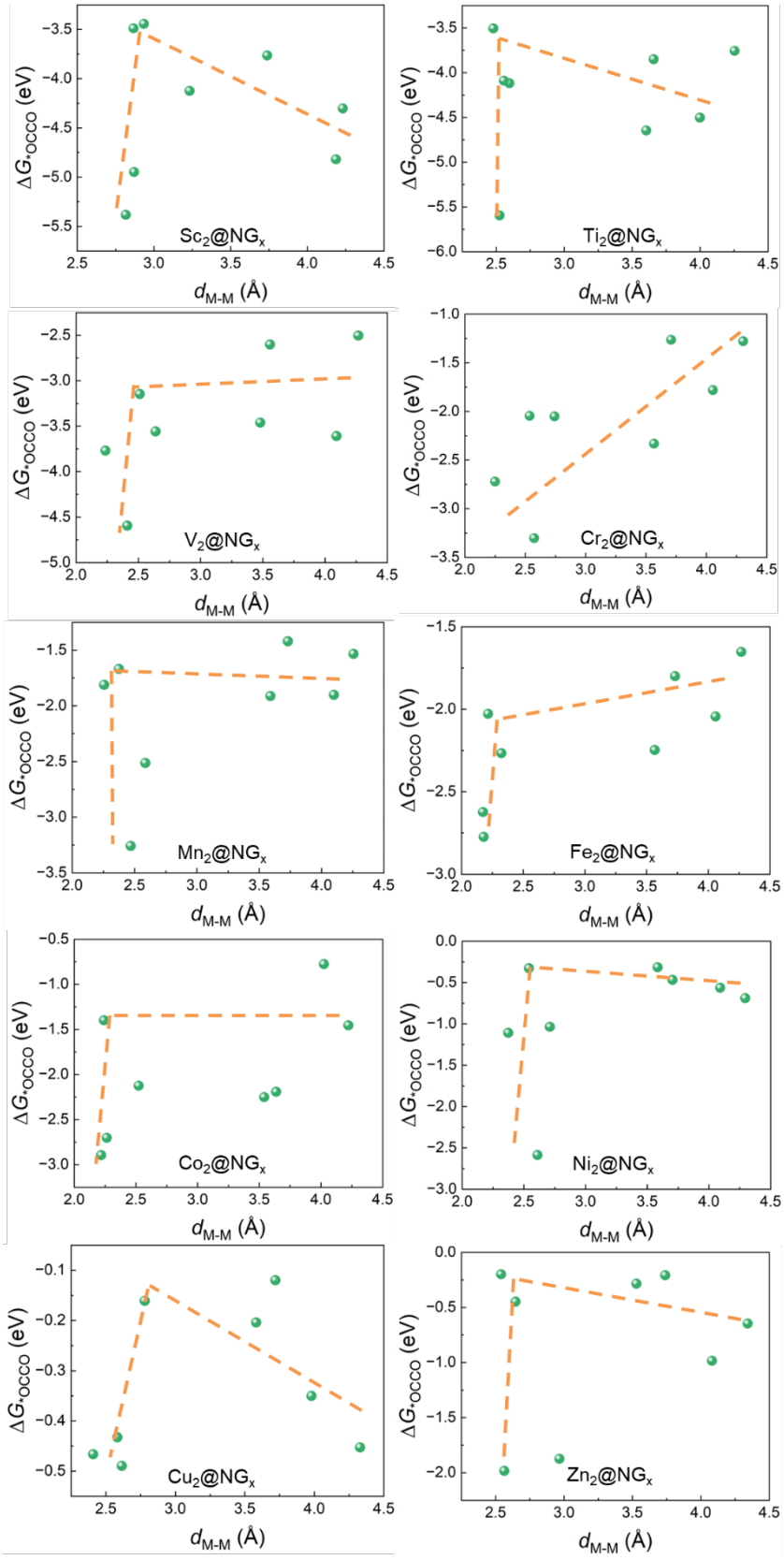

Figure S22. Adsorption energies of *OCCO molecules as a function of metal−metal distance in $M_2@NG_x$.

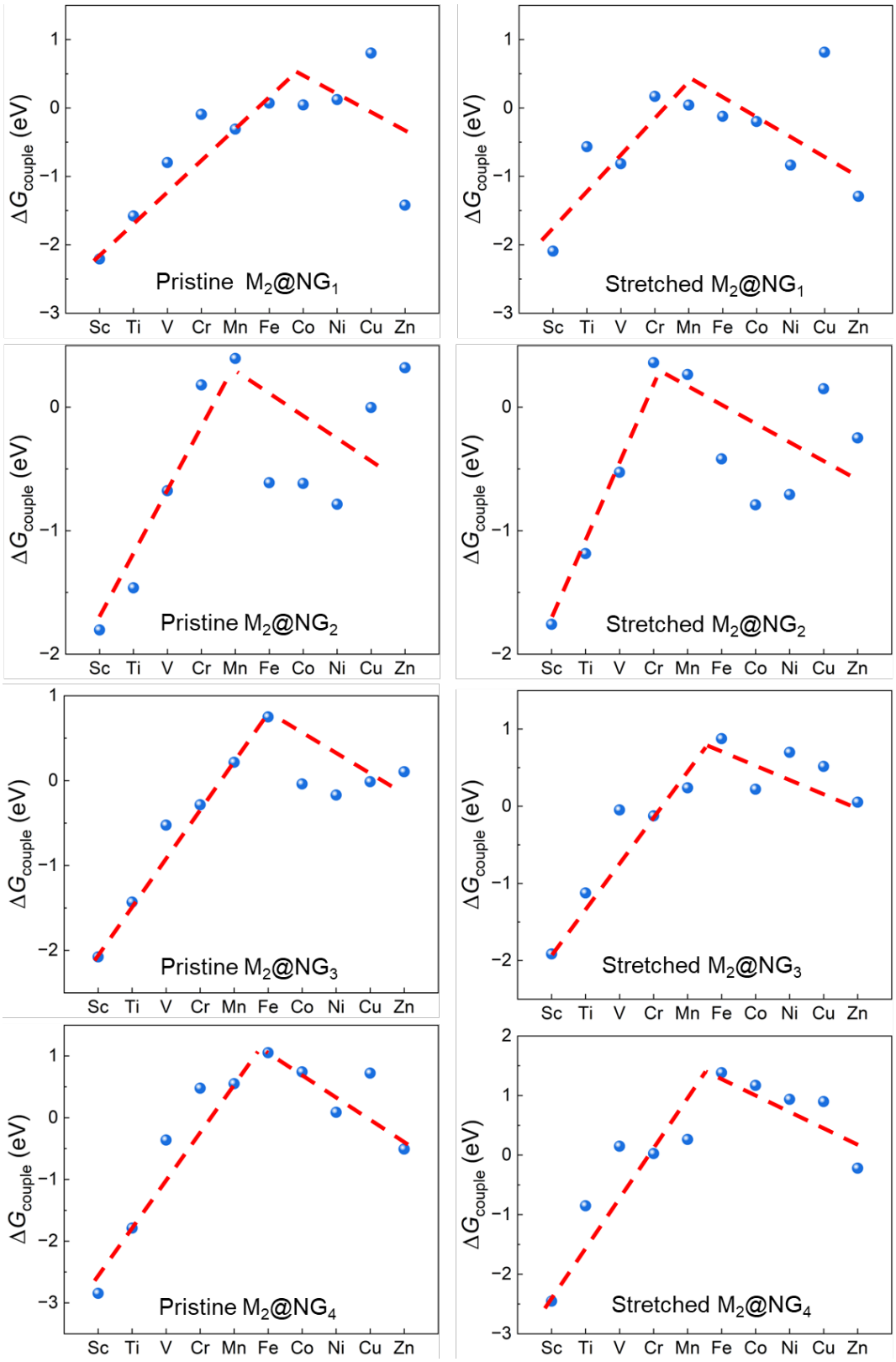

Figure S23. C−C coupling energies as a function of metal identity in $M_2@NG_X$.

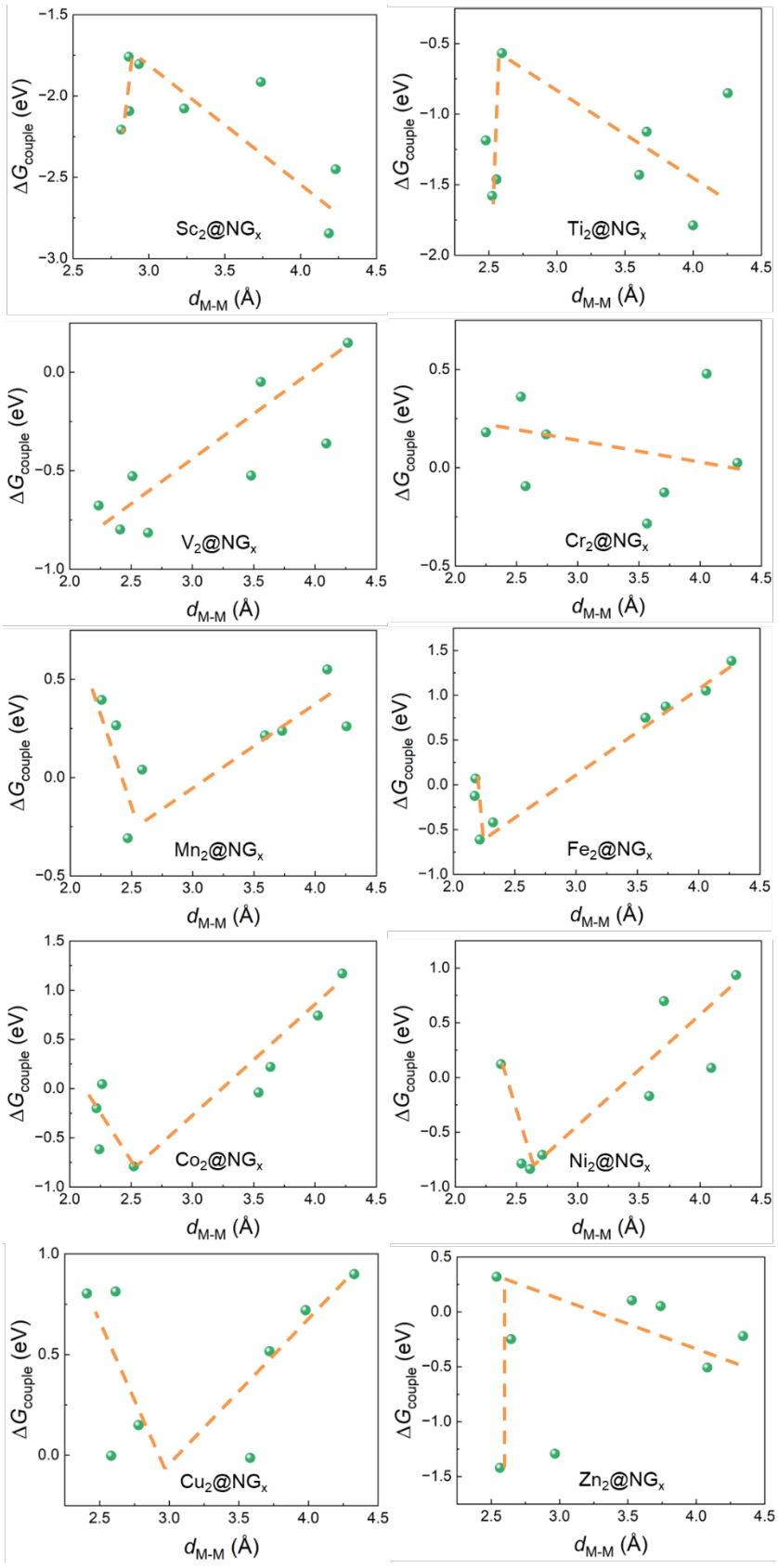

Figure S24. C−C coupling energies as a function of metal−metal distance in $M_2@NG_x$.

Table S11. Primary features used in this work.

Symbol	Physical meaning	Symbol	Physical meaning
$N_{\mathrm{M}}^{\mathrm{VE}}$	Number of metal valence electrons	$R_{\mathrm{M}}^{\mathrm{CR}}$	Covalent radius of metal
$N_{\mathrm{M}}^{\mathrm{men}}$	Mendeleev number of metal[1]	$R_{\mathrm{M}}^{\mathrm{vdw}}$	Van der Waals radius of metal
$N_{\mathrm{M}}^{\mathrm{group}}$	Group of metal	$R_{\mathrm{M}}^{\mathrm{atom}}$	Atomic radius of metal
$N_{\mathrm{M}}^{\mathrm{atom}}$	Atomic number of metal	$R_{\mathrm{M}}^{\mathrm{ion}}$	Ionic radius of metal
$E_{\mathrm{M}}^{\mathrm{ion}}$	First ionization energy of metal	$N_{\mathrm{N}}^{\mathrm{dop}}$	The number of N dopants in the support
$E_{\mathrm{M}}^{\mathrm{EA}}$	Electronic affinity of metal	$N_{\mathrm{MN}}^{\mathrm{coor}}$	N coordination number of metal
χ_{M}	Pauling electronegativity of metal	d_{MM}	Metal−metal distance
$C_{\mathrm{M}}^{\mathrm{TC}}$	Thermal conductivity of metal	S_{ratio}	Stretching ratio of catalyst

[1] Villars, P.; Cenzual, K.; Daams, J.; Chen, Y.; Iwata, S., Data-driven atomic environment prediction for binaries using the Mendeleev number: Part 1. Composition AB. Journal of Alloys and Compounds 2004, 367 (1), 167-175.

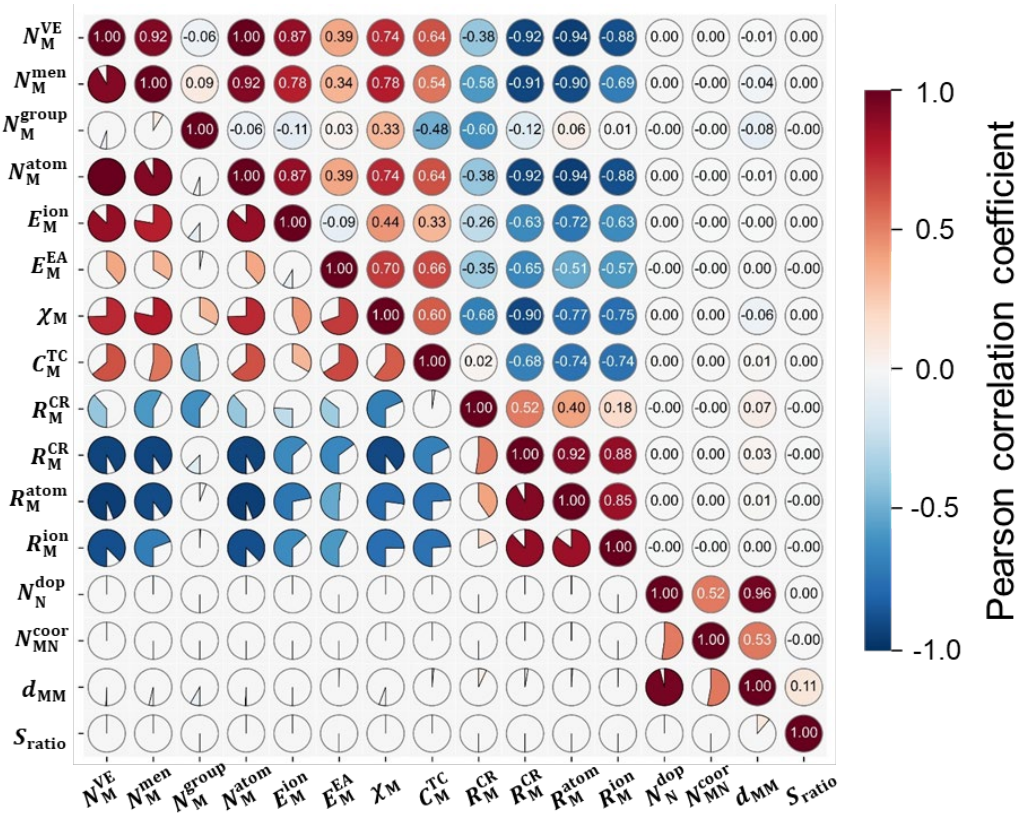

Figure S25. Pearson correlation coefficients among all primary features.

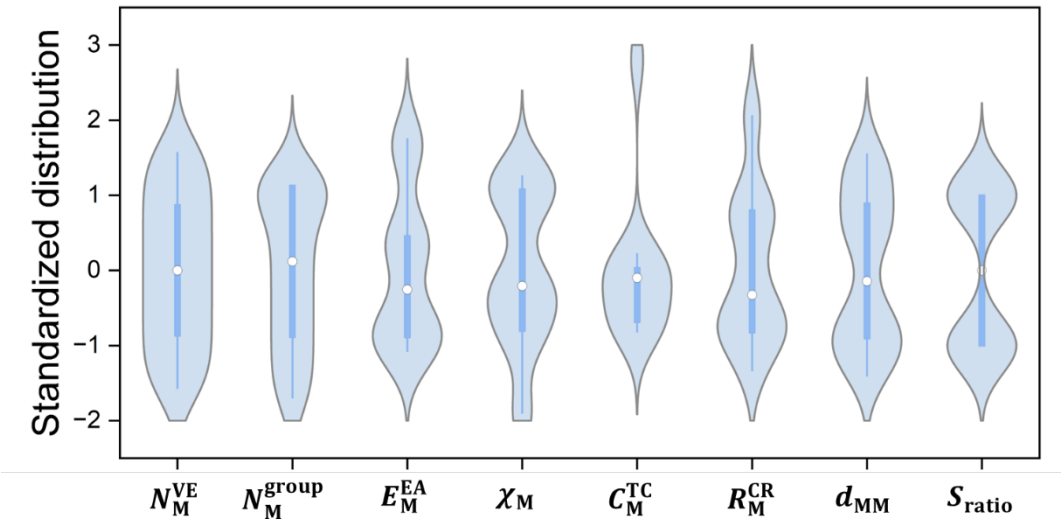

Figure S26. Pearson correlation coefficients among all screened primary features.